IEEE Access
Multidisciplinary | Rapid Review | Open Access Journal

Received 31 August 2023, accepted 29 September 2023, date of publication 4 October 2023, date of current version 10 October 2023.

Digital Object Identifier 10.1109/ACCESS.2023.3321670

RESEARCH ARTICLE

Single-User SFLC-OFDM System Realization Based on Channel Reciprocity Recovery

SUBIN KIM[1], HAN-GYEOL LEE[2], (Student Member, IEEE), SONGMIN LEE[1], JAEHONG KIM[2], (Student Member, IEEE), JINGON JOUNG[2], (Senior Member, IEEE), AND JUYEOP KIM[1], (Member, IEEE)

[1]Department of Electronics Engineering, Sookmyung Women's University, Seoul 04312, South Korea
[2]School of Electrical and Electronics Engineering, Chung-Ang University, Seoul 06974, South Korea

Corresponding authors: Jingon Joung (jgjoung@cau.ac.kr) and Juyeop Kim (jykim@sookmyung.ac.kr)

This work was supported by the Institute of Information and Communications Technology Planning and Evaluation (IITP) Grant funded by the Korea Government [Ministry of Science and ICT (MSIT)] under Grant 2021-0-00874.

ABSTRACT This paper demonstrates the implementation of a space–frequency line coded-orthogonal frequency-division multiplexing (SFLC-OFDM) system. The SFLC-OFDM system utilizes downlink channel state information at the transmitter, which can be obtained from uplink channel estimation under channel reciprocity assumption between uplink-and-downlink channels. However, in practical implementations, channel reciprocity is violated due to the imperfect synchronization and radio frequency chain mismatch between transceivers. To recover the channel reciprocity, frequency-domain signal processing methods are proposed. Furthermore, a low computational complexity single-instruction multiple-data method is implemented to meet the time constraints in real-time operating systems. The experimental results demonstrate that channel reciprocity can be effectively recovered in the implemented SFLC-OFDM system, resulting in practical communication performance regarding the symbol error rate.

INDEX TERMS Space–frequency line code (SFLC), orthogonal frequency-division multiplexing (OFDM), synchronization, channel reciprocity, software-defined radio (SDR), single-instruction multiple-data (SIMD) method.

I. INTRODUCTION

As the fifth generation (5G) terminal devices continue to expand their applications, many researchers have begun to consider the next-generation mobile communication system, commonly referred to as the sixth generation (6G) [1], [2]. Multiple-input multiple-output (MIMO) systems have emerged as an essential technology expected to deliver significant performance enhancements in 6G by leveraging spatial diversity and multiplexing gains [3]. Thus, the MIMO techniques have been applied to the various communication systems, such as massive MIMO systems [4], [5], [6], multi-user MIMO (MU-MIMO) systems [7], [8], [9], [10], and cell-free MIMO systems [11], [12], [13], [14]. These MIMO systems have shown noticeable performance improvement in spectral and energy efficiency.

The associate editor coordinating the review of this manuscript and approving it for publication was Nurul I. Sarkar.

One of the critical technologies determining the performance of MIMO systems is the channel state information (CSI) estimation techniques [15], [16], [17]. In frequency-division duplexing (FDD) systems, downlink (DL) CSI from a base station (BS) to users is desired to exploit various advanced MIMO techniques, such as MU-MIMO, beamforming, and scheduling, to improve the DL communication performance in 6G systems. To this end, the DL CSI should be fed back from the users to the BSs, even though the BS has uplink (UL) CSI from the UL channel estimation. This is because the UL can DL channels are not reciprocal in the FDD systems [18], [19], [20], [21].

To circumvent the feedback overhead in the FDD systems, time-division duplexing (TDD) systems were vigorously studied [22], [23], [24], [25], [26], [27], [28]. Since the transceiver operates in a single frequency band in TDD systems, the DL/UL channel responses are reciprocal, i.e., the channel reciprocity/symmetry. The DL channel can be

estimated via UL training based on the symmetric channel between DL and UL, and the feedback overhead issue can be resolved. However, owing to a massive number of transmit antennas recently considered in 6G BSs to support explosively growing data traffic, the pilot overhead to estimate DL CSI can be prohibitively increased [29]. In other words, the tremendous DL signaling overhead may hinder 6G BS from being deployed in practice.

To reduce the DL signaling overhead, which is for the DL channel estimation at the users (henceforth denoted by a receiver, RX), a space–time line code (STLC) scheme [30] is employed at the BS (henceforth denoted by a transmitter, TX). The STLC is a space-time coding scheme that can gain full spatial diversity with CSI at TX (CSIT) operating in a TDD mode. Concretely, the STLC TX encodes the data symbols using CSIT, and the STLC RX decodes them without or with partial CSI at RX (CSIR). To show the validity of STLC, several studies were conducted on the theoretical aspects [31], [32], [33], [34], [35]. For these advantages, the STLC has been applied to various communication systems, such as MU-MIMO systems [36], [37], [38], multi stream MIMO systems [39], [40], multicast system [41], secure communication systems [42], [43], relay communication systems [44], [45], [46], [47], intelligent reflecting surface systems [48], [49], vehicular communication systems [50], Unmanned vehicle communication systems [51], [52], and non-orthogonal multiple access systems [53], [54]. The STLC scheme was employed in an orthogonal frequency division multiplexing (OFDM) system, i.e., a space–frequency line code (SFLC) system [55]. A real-time operating testbed was implemented due to the simple modem structure of SFLC.

Previous STLC (or SFLC) studies assumed perfect UL and DL channel reciprocity. However, an undesirable asymmetry exists between the DL and UL channels [56], [57]. To guarantee the channel reciprocity in the TDD systems, the hardware calibration methods have been proposed [58], [59], [60], [61], [62], [63], [64], which can match the radio frequency (RF) responses of TX and RX. However, the residual frequency and timing offset still cause significant impairment in the phase of channel frequency response (CFR) [65, Ch. 5, pp. 105–110]. Therefore, further signal processing methods are necessary to compensate for the residual timing and frequency offsets.

This paper proposes a frequency-domain synchronization method to guarantee the reciprocal channel responses between DL and UL of a TDD SFLC-OFDM system. Furthermore, the real-time operating software-defined radio (SDR) testbed is implemented. The proposed methods, including the SFLC encoder and decoder, are designed using a single-instruction multiple-data (SIMD) technique to satisfy the time constraints in real-time systems. The main contributions of this paper are summarized as follows:

1) Frequency-domain signal processing methods are proposed to compensate for the residual timing and frequency offset, namely symbol timing offset (STO) and carrier frequency offset (CFO), of the implemented single-user TDD SFLC-OFDM system. As a result, the phase difference between DL/UL CFRs can be effectively eliminated.
2) The designed SFLC-OFDM system is implemented in the SDR environment. To make the SFLC system feasible in the universal software radio peripheral (USRP) devices, the proposed signal processing methods are designed to minimize floating-point operations (FLOPS) and the non-linear function call.
3) The performance of the SFLC-OFDM system is evaluated through the hardware experiment in the practical environment. It is verified that channel reciprocity can be attained using the proposed methods. Moreover, the implemented SFLC-OFDM system outperforms the conventional SISO-OFDM system's symbol error rate (SER) performance.

The remainder of this paper is organized as follows. Section II describes the TDD SFLC-OFDM system model, including the TDD frame structure and signal models of STO, CFO, and RF mismatch. The proposed algorithms for channel reciprocity are presented in Section III. The experimental results are demonstrated in Section IV to verify the proposed methods and implementation of SFLC-OFDM. Finally, Section V provides the conclusion of this paper.

Notations: Scalars, vectors, and matrices are denoted by lowercase, boldface lowercase, and boldface capital letters, e.g., x, $\mathbf{x}$, and $\mathbf{X}$, respectively. $\mathbf{x}[n]$ represent the nth element of $\mathbf{x}$; $\mathbf{x}[m : n]$ denotes the vector including from the mth to nth elements of $\mathbf{x}$. Superscript $*$ denotes complex conjugate for any scalar, vector, or matrix. $\otimes$ and $\oplus$ denote the element-wise multiplication and addition between two vectors.

II. SYSTEM AND SIGNAL MODELS

Fig. 1 illustrates the single user 1×2 TDD SFLC-OFDM system [55]. In DL, the BS and the user equipment (UE) in DL operate as TX and RX, respectively. The BS encodes data bits to SFLC symbols. Then, the SFLC and preamble symbols are allocated to the corresponding subcarriers. The time-domain baseband OFDM signals are transmitted from the BS to the UE through the wireless channel. The UE uses the received time-domain preamble signals to synchronize frame timing and carrier frequency. Then, the data bits are estimated after SFLC decoding.

The BS and UE operate as RX and TX in UL. The UE allocates the pilot and preamble symbols to the corresponding subcarriers. The OFDM baseband signals, including the preamble and pilot, are transmitted to the BS. Similarly to the DL, the BS achieves frame timing and carrier frequency synchronizations. The UL channels between the two UE antennas and a single BS antenna are estimated using received pilot symbols. The estimated channels are used for the SFLC encoding in the subsequent DL communication.

The TDD frame structure is represented in Fig. 2. One frame consists of four slots. The DL and the UL slots alternate

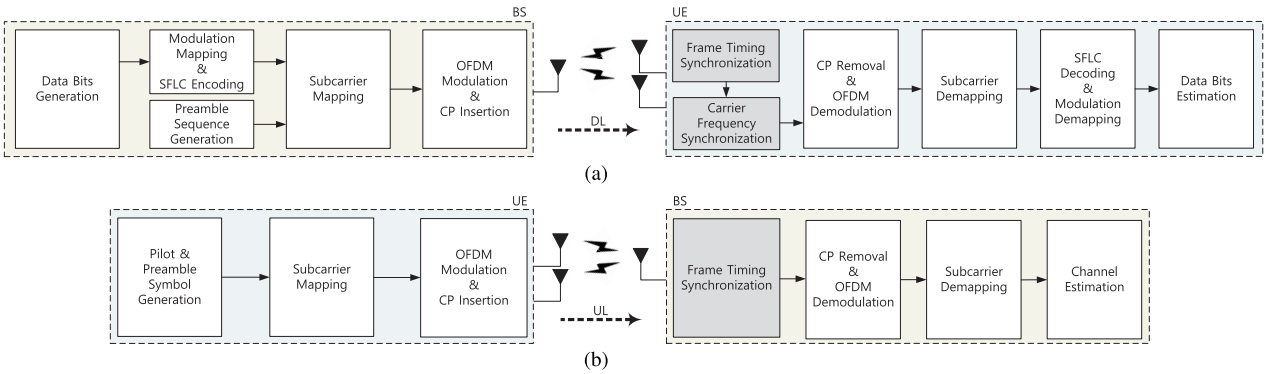

FIGURE 1. SFLC-OFDM system block diagram. (a) DL mode. (b) UL mode.

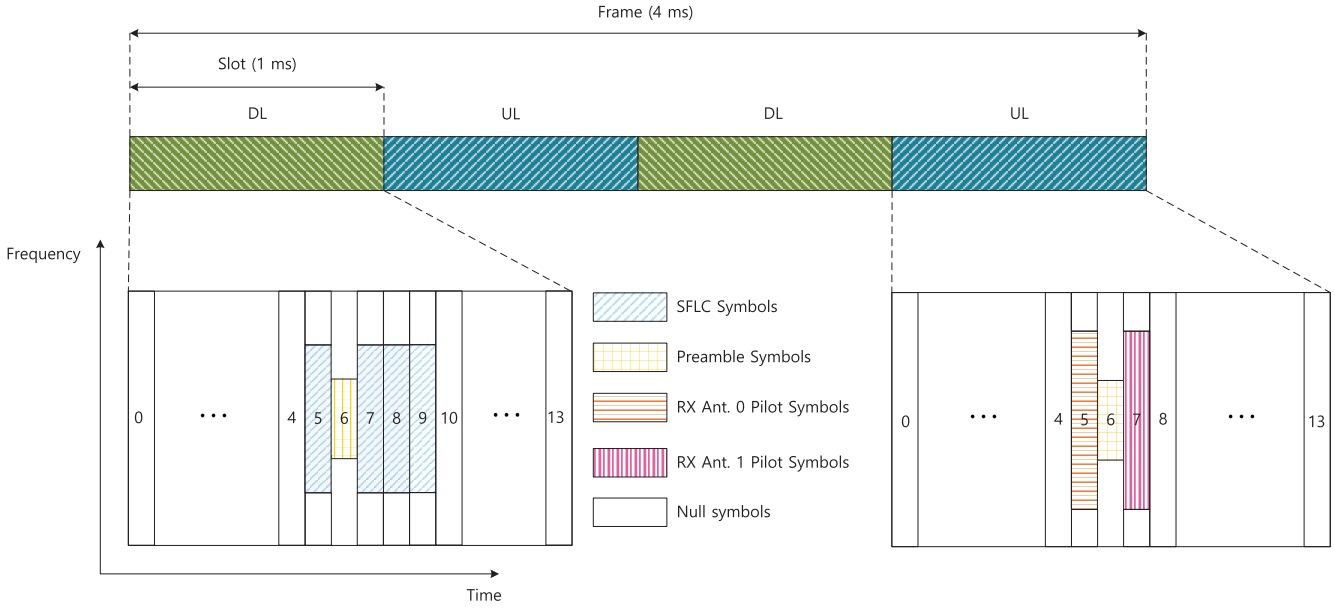

FIGURE 2. Frame structure for TDD communication.

in one frame. The duration of slot and frame are one and four milliseconds, respectively. One slot consists of 14 OFDM symbols. The preamble symbols are allocated to the sixth OFDM symbol in the DL slot. The SFLC symbols are transmitted through the fifth and from the seventh to the ninth OFDM symbols. No signals are transmitted during the first five and last four OFDM symbols to guarantee the marginal time for DL/UL switching. In the UL slot, the preamble is assigned to the sixth OFDM symbol in the same manner as the DL. The pilot symbols are allocated to the fifth (seventh) OFDM symbol for the zeroth (first) UE antenna. Similarly, no signals are transmitted with the DL slot through the first five and last six OFDM symbols for DL/UL switching.

A. OPERATIONS IN DL AND UL COMMUNICATIONS

The BS allocates preamble symbols to the sixth OFDM symbol in each DL slot. The SFLC symbols are transmitted through the fifth, and from the seventh to the ninth OFDM symbols. In SFLC-OFDM systems, the two data symbols are SFLC encoded as follows [55]:

$$\begin{bmatrix} X_k^* \\ X_{k+1} \end{bmatrix} = \frac{1}{\sqrt{|H_{0,k}|^2 + |H_{1,k}|^2}} \begin{bmatrix} H_{k,0} & H_{k,1} \\ H_{k,0}^* & -H_{k,1}^* \end{bmatrix} \begin{bmatrix} D_k \\ D_{k+1} \end{bmatrix}, \tag{1}$$

where D_k and X_k are the kth data and SFLC symbol, respectively. In this paper, D_k is assumed to be a phase shift keying (PSK) modulated symbol where no CSIR is required for the SFLC decoding [30]. $H_{k,i}$ is the k subcarrier CFR between the ith UE and BS antennas. It is assumed that $H_{k,i} \approx H_{k+1,i}$ [55], and the channel is static over the two slot duration and Rician fading. Then, $H_{k,i}$ is written as follows [66]:

$$H_{i,k} = H_i^{\mathrm{LOS}} + H_{k,i}^{\mathrm{SCA}}, \tag{2}$$

where H_i^{LOS} and $H_{k,i}^{\mathrm{SCA}}$ are the line-of-sight (LOS) and multipath scatter component of $H_{k,i}$, respectively. H_i^{LOS} is

an arbitrary constant; $H_{k,i}^{\mathrm{SCA}}$ is zero-mean complex Gaussian random variable whose the variance σ_H^2 is determined by the K-factor.

Let $\mathcal{N}^{\mathrm{d}} = \{-d/2, \ldots, -1, 1, \ldots, d/2\}$ denote the data subcarrier index set for the number of data subcarrier d. The baseband OFDM signals for data transmission are written as follows [65, Ch. 5, p. 130]:

$$x_n = \frac{1}{\sqrt{N}} \sum_{k \in \mathcal{N}^{\mathrm{d}}} X_k e^{j2\pi \frac{nk}{N}}, n \in \{0, 1, \ldots, N-1\}, \quad (3)$$

where x_n is the nth OFDM sample in time domain and N is the fast Fourier transform size.

For the preamble transmission, the primary synchronization signal of 5G standard is used whose length is 127 [67]. The preamble symbols are allocated to the DC subcarrier and either side. No SFLC symbol is transmitted with the preamble symbols for accurate timing and frequency synchronization. Thus, the baseband OFDM signals for preamble transmission are written as follows:

$$s_n = \frac{1}{\sqrt{N}} \sum_{k=-63}^{63} S_k e^{j2\pi \frac{nk}{N}}, n \in \{0, 1, \ldots, N-1\}, \quad (4)$$

where s_n and S_k are the nth and kth preamble sample and symbol in the time and frequency domain, respectively. Here, $S_k \in \{-1, 1\}$ [67]. After cyclic prefix (CP) insertion to each OFDM symbol, the DL slot is transmitted to the UE.

In the initial acquisition stage, the UE synchronizes the received signals using preambles through the zeroth UE antenna. The frame timing offset $\hat{\delta}$ is estimated from the correlation between transmitted and received preamble signals as follows [68]:

$$\hat{\delta} = \arg\max_{\delta} \left| \sum_{n=0}^{N-1} s_n^* r_{n+\delta,0} \right|, \quad (5)$$

where $r_{n,0}$ is the nth sample of the OFDM symbol, including the preamble signals and CP received through the zeroth UE antenna. Then, the CFO is estimated as follows [68]:

$$\hat{\theta} = \frac{1}{\pi} \angle \left(\left[\sum_{n=0}^{N/2-1} s_n^* r_{n+\hat{\delta},0} \right] \left[\sum_{n=N/2}^{N-1} s_n^* r_{n+\hat{\delta},0} \right] \right), \quad (6)$$

where $\hat{\theta} \in (-1, 1)$ is the estimated normalized CFO. Using $\hat{\delta}$ and $\hat{\theta}$, UE performs the frame and frequency synchronization [68].

After synchronization and CP removal, the kth SFLC symbol received through the ith UE antennas, denoted by $Y_{k,i}$, is given as

$$Y_{k,i} = \frac{1}{\sqrt{N}} \sum_{n=0}^{N-1} y_{n,i} e^{-j2\pi \frac{nk}{N}}, k \in \mathcal{N}^{\mathrm{d}}, \quad (7)$$

where $y_{n,i}$ is the nth sample of OFDM signals including SFLC sybmols received through the ith UE antenna. Using $Y_{k,i}$, the received data symbols are written as follows [55]:

$$\begin{bmatrix} \hat{D}_k \\ \hat{D}_{k+1} \end{bmatrix} = \begin{bmatrix} Y_{k,0}^* + Y_{k+1,1} \\ Y_{k+1,1}^* - Y_{k+1,0} \end{bmatrix}. \quad (8)$$

The data bits are demodulated from $\{D_k\}$ through the PSK demapping.

To conduct SFLC encoding in the DL, the CSIT is required [30]. To this end, the UE transmits the preamble and pilot symbols in the UL slot. The BS synchronizes the received signals using preambles and estimates channels with pilot symbols. In the UL, the preamble symbols are transmitted in the same way as the DL. Thus, we omit the details of the UL preamble transmission.

For the pilot symbol transmission, the demodulation reference signal of 5G standard is used [67]. Let $\mathcal{N}_i^{\mathrm{p}}$, $i \in \{0, 1\}$, denote the pilot subcarrier index set involved with the ith UE antenna. The pilot symbols of the ith UE antenna are mapped to the subcarriers in $\mathcal{N}_i^{\mathrm{p}}$. Then, the baseband OFDM signals, including pilot and preamble symbols, are transmitted after the CP insertion. Since CFO is compensated in the previous DL, the BS conducts only frame synchronization using the received preamble signals as in (5). Then, the CFRs between the ith UE and BS antennas are estimated with the least square method as follows [69]:

$$\hat{H}_{k,i} = Q_{k,i} P_{k,i}^*, \quad k \in \mathcal{N}_i^{\mathrm{p}}, \quad (9)$$

where $P_{k,i}$ and $Q_{k,i}$ are the kth transmit and received pilot symbols involved with the ith UE antenna, respectively. $\hat{H}_{k,i}$ is the estimated CFR of the kth pilot subcarrier between the ith UE and BS antennas. To obtain the CFR of subcarriers in $\mathcal{N}^{\mathrm{d}}$, the linear interpolation is applied to $\{\hat{H}_{k,i}\}$ with respect to k for each i [70, Ch. 6, p. 193]. The estimated UL CFRs are used for the DL SFLC encoding in (1).

B. EFFECT OF IMPERFECT SYNCHRONIZATION AND RF CHAIN

At each initial acquisition in the DL and UL, the RX achieves the frame timing at the initial acquisition in the DL and UL. However, the RX fails to estimate the correct timing and frequency offset due to the impairments such as additive noise, sampling clock offset (SCO), and phase noise [71]. As a result, residual timing and frequency offsets are present in the received signals. These offsets usually differ in the DL and UL communications and jeopardize channel reciprocity. In the presence of residual timing offset, the received symbols in the frequency domain experience phase rotation proportional to the subcarrier index. Since the residual CFO is considerably small after initial frequency synchronization, its effect can be represented as the phase offset [70, Ch. 5, p. 161].

In addition to the imperfect synchronization, the channel reciprocity also breaks down due to the asymmetric RF chain response in DL and UL [72]. Theoretically, the RF chain response is frequency dependent. However, it is observed that the frequency dependency is negligible from the experimental results of the implemented testbed. Thus, we adopt the

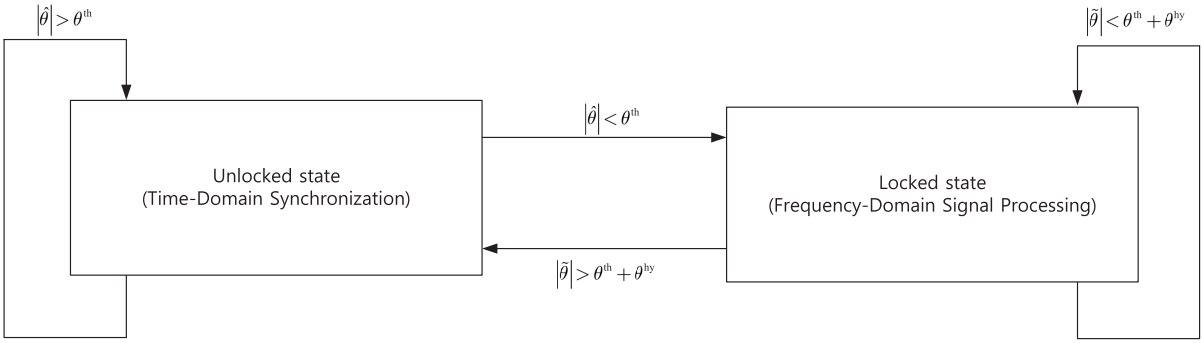

FIGURE 3. State transition of proposed two-states CFO estimation method.

frequency-independent RF chain response model, which can be written as a single complex coefficient. This study assumes that amplitude calibration between the BS and two UE antennas is achieved before communication. Then, the effect of asymmetric UL and DL RF chain response is represented as a relative phase offset between the ith UE and BS antennas.

The received SFLC and pilot symbols with imperfect synchronization and RF chain are approximated as follows:

$$Y_{k,i} \approx X_k \underbrace{\left(H_{k,i} e^{jk\phi^{\text{DL}}}\right)}_{\text{effective DL CFR}} + W_{k,i}^{\text{DL}}, \ k \in \mathcal{N}^{\text{d}}, \tag{10a}$$

$$Q_{k,i} \approx P_{k,i} \underbrace{\left(H_{k,i} e^{jk\phi^{\text{UL}}} e^{j\psi_i^{\text{UL}}}\right)}_{\text{effective UL CFR}} + W_{k,i}^{\text{UL}}, \ k \in \mathcal{N}_i^{\text{p}}, \tag{10b}$$

where ϕ^{DL} and ϕ^{UL} are the phase rotation due to residual timing offset in DL and UL, respectively. ψ_i^{UL} is relative phase offset between the ith UE and BS antennas in UL. $W_{k,i}^{\text{DL}}$ and $W_{k,i}^{\text{UL}}$ are additive noise terms in DL and UL, respectively, involved with the ith UE antenna. It is assumed that $W_{k,i}^{\text{DL}}$ and $W_{k,i}^{\text{UL}}$ are zero-mean complex Gaussian random variables with the variance σ_w^2. In (10), it is readily shown that the phase discrepancy is present between the effective DL and UL CFRs, resulting in the non-reciprocal channel.

III. PROPOSED SIGNAL PROCESSING METHODS FOR RECOVERING CHANNEL RECIPROCITY

Under imperfect synchronization and asymmetric DL/UL RF chain responses, the phase difference between UL and DL CFRs is represented as multiplicative distortion. Typically, the multiplicative distortion can be compensated by channel estimation in OFDM systems with CSIR [73], [74]. As a result, the single-input single-output (SISO) and 2×2 MIMO space-frequency block coded OFDM systems are implemented without phase distortion compensation [75], [76]. However, the phase discrepancy should be compensated in OFDM systems with CSIT to attain channel reciprocity. To this end, a two-state-based SFLC-OFDM system and frequency-domain signal processing methods are proposed in this section. Then, the considerations for SDR implementation of real-time operating SFLC-OFDM system are described.

A. TWO-STATE-BASED SFLC-OFDM SYSTEM

As shown in (10), the phase distortion is present in the frequency domain. An additional frequency-domain signal processing procedure is necessary to compensate for these phase terms. However, the CFO usually has a large value at the initial stage of communication. In this case, any signal processing in the frequency domain can not be performed due to severe CFO-induced inter-carrier interference [70, Ch. 5, p. 161]. Thus, the UE and BS should determine whether the frequency-domain signal processing can be appropriately conducted under the current CFO. For this end, we design the two states-based SFLC-OFDM system.

Fig. 3 illustrates the state transition in the proposed two states-based SFLC-OFDM system. θ^{th} and θ^{hy} are the threshold and hysteresis value, respectively. In the initial stage of communication, the states of UE and BS are initialized as unlocked states. At the unlocked state, other signal processing (namely SFLC encoding, decoding, channel estimation, and phase distortion estimation) is not conducted; yet, UE compensates the CFO using $\hat{\theta}$ in every DL slot. In each DL/UL slot, RX compares $\hat{\theta}$ in (5) with θ^{th}. If $\hat{\theta} > \theta^{\text{th}}$ at the unlocked state, RX determines that the current CFO is too large for stable communication. No state transition occurs in this case. Otherwise, the state changes from unlocked to locked. Then, further signal processing is performed in the frequency domain. Similarly, the state is set to unlocked if $\hat{\theta} > \theta^{\text{th}} + \theta^{\text{hy}}$ at the locked state. Here, θ^{hy} is used to avoid carrier frequency fluctuation.

B. PHASE ROTATION ESTIMATION

The residual timing offset can be estimated by computing a slope from the plot of received preamble symbol phase differences versus the corresponding subcarrier indices [65, Ch. 6, p. 147]. The average of phase differences between the adjacent two preamble symbols can be used to estimate the slope corresponding to phase rotation [65, Ch. 6, p. 148]. However, this method requires several argument function invocations, which is burdensome for the real-time operating

SDR implementation. Furthermore, the additive noise term can only be converted to the equivalent zero-mean phase noise under the high SNR assumption [77]. Otherwise, the zero mean of phase noise terms is not guaranteed. In other words, the equivalent phase noise terms due to the additive noise are not averaged out in the low and intermediate SNR regimes. The direct averaging method of phase differences has limited noise suppression capability. To resolve these problems, we proposed the slope estimation method using two partial average terms of estimated CFR. The phase rotation is assumed to be estimated using the received signals with the zeroth UE antenna in DL without loss of generality. The proposed phase distortion estimation method is identically conducted at the UE and BS and in every DL/UL slot when the state is locked. Thus, we omit UE antenna index i for notational simplicity and the superscripts UE and BS in Section III-B.

The average channel response corresponding to the lower- and upper-frequency bands of the preamble symbol can be written as follows:

$$\begin{aligned}\bar{H}^{\text{low}} &= \frac{1}{63}\sum_{k=-63}^{-1} R_k S_k^* \\ &= \frac{1}{63}\sum_{k=-63}^{-1} (H^{\text{LOS}} + H_k^{\text{SCA}})|S_k|^2 e^{j(k\phi+\psi)} + W_k S_k^* \\ &= e^{-j64\phi} H^{\text{LOS}} e^{j\psi}\left(\frac{1}{63}\sum_{k=1}^{63} e^{jk\phi}\right) + Z^{\text{low}}, \end{aligned} \tag{11a}$$

$$\begin{aligned}\bar{H}^{\text{up}} &= \frac{1}{63}\sum_{k=1}^{63} R_k S_k^* \\ &= \frac{1}{63}\sum_{k=1}^{63} (H^{\text{LOS}} + H_k^{\text{SCA}})|S_k|^2 e^{j(k\phi+\psi)} + W_k S_k^* \\ &= H^{\text{LOS}} e^{j\psi}\left(\frac{1}{63}\sum_{k=1}^{63} e^{jk\phi}\right) + Z^{\text{up}}, \end{aligned} \tag{11b}$$

where R_k is the kth received preamble symbol. Z^{low} and Z^{up} are the multipath scatter component plus noise terms given by

$$Z^{\text{low}} = \frac{1}{63}\sum_{k=-63}^{-1} H_k^{\text{SCA}} e^{j(k\phi+\psi)} + W_k S_k^*, \tag{12a}$$

$$Z^{\text{up}} = \frac{1}{63}\sum_{k=1}^{63} H_k^{\text{SCA}} e^{j(k\phi+\psi)} + W_k S_k^*. \tag{12b}$$

Here, it can be readily shown that Z^{low} and Z^{up} are the zero-mean complex Gaussian with the variance $\sigma_z^2 = \frac{1}{63}(\sigma_H^2 + \sigma_w^2)$. Assuming that Z^{low} and Z^{up} are averaged out, i.e., $\sigma_z^2 \approx 0$, $\bar{H}^{\text{low}}$ is reduced to $e^{-j64\phi}\bar{H}^{\text{up}}$. Thus, the slope can be estimated as follows:

$$\hat{\phi} = \frac{1}{64}\angle\left(\bar{H}^{\text{up}}\bar{H}^{\text{low},*}\right). \tag{13}$$

The phase rotation is compensated by multiplying $e^{-jk\hat{\phi}}$ to the received symbol whose subcarrier index is k.

C. PHASE OFFSET ESTIMATION

After phase rotation compensation, the relative phase offset is estimated at the BS in UL. At first, BS estimates the average of UL CFR between the zeroth UE and BS antenna using the received preamble as follows:

$$\bar{H}_0^{\text{UL}} = \frac{1}{127}\sum_{k=-63}^{63} R_k^{\text{UL}} S_k^*, \tag{14}$$

where superscript UL is used to indicate that R_k^{UL} is the kth preamble symbol in UL. Then, the average UL CFR phase difference between the two UE and BS antennas is computed as

$$H^{\text{diff}} = \frac{\tilde{H}_0^{\text{UL},*}\tilde{H}_1^{\text{UL}}}{\left|\tilde{H}_0^{\text{UL},*}\tilde{H}_1^{\text{UL}}\right|}, \tag{15a}$$

$$\tilde{H}_i^{\text{UL}} = \sum_{k\in\mathcal{N}_i^{\text{p}}} Q_{k,i} P_{k,i}^*, \tag{15b}$$

where $\tilde{H}_i^{\text{UL}}$ is the sum of estimated CFR between the ith UE and BS antennas. Since phase offset is independent of the subcarrier index, the relative phase offset terms can be estimated from the phase of average UL CFR between the UE and BS antennas. Thus, BS estimates ψ_i^{UL} as follows:

$$\hat{\psi}_0^{\text{UL}} = \angle\left(\bar{H}_0^{\text{UL}}\right), \tag{16a}$$

$$\hat{\psi}_1^{\text{UL}} = \angle\left(\bar{H}_0^{\text{UL}} H^{\text{diff}}\right). \tag{16b}$$

By multiplying $e^{j\hat{\psi}_i^{\text{UL}}}$ to $\hat{H}_{k,i}$ in (9), the relative phase offsets between two UE and BS antennas are compensated.

D. FINE CFO ESTIMATION

The time-domain correlation-based CFO estimation method typically has a relatively large residual CFO. However, it is robust to the noise and has a large range of estimable frequency offset [68]. Furthermore, carrier frequency fluctuation occurs in the CFO tracking stage due to its limited estimation performance. To resolve the aforementioned problems, a frequency-domain CFO estimation method is necessary, typically referred to as fine frequency synchronization [78]. For this end, the fine CFO estimation method is proposed using the preamble symbols of the two successive DL slots. In the tth DL slot, UE computes the average CFR of the preamble symbols received through the zeroth UE antenna as follows:

$$\bar{H}_{0,t}^{\text{DL}} = \frac{1}{127}\sum_{k=-63}^{63} R_{k,0,t}^{\text{DL}} S_k^*, \tag{17}$$

where $R_{k,0,t}^{\text{DL}}$ is the kth received preamble symbols with the zeroth UE antenna in the tth DL slot. Assuming that the multipath scatter component plus noise terms are averaged

out, the LOS component is dominant in (17). In the presence of a CFO, the phase variation of CFR over two successive DL slots is $2\pi\theta\Delta t\Delta f$ [79]. Here, Δt and Δf denote the time interval between two consecutive DL slots and subcarrier spacing, respectively. The LOS term is generally static over a long time in fixed point-to-point communication systems. Thus, the phase variation is the phase shift corresponding to the residual CFO, i.e., $\bar{H}^{\mathrm{DL}}_{0,t} \approx e^{j2\pi\theta\Delta t\Delta f}\bar{H}^{\mathrm{DL}}_{0,t-1}$. From the phase difference between the two average CFRs of successive DL slots, the residual CFO can be estimated as follows:

$$\tilde{\theta} = \frac{\angle\left(\bar{H}^{\mathrm{DL}}_{0,t}\bar{H}^{\mathrm{DL},*}_{0,t-1}\right)}{2\pi\,\Delta t\Delta f}. \tag{18}$$

Depending on the current state, the UE compensates the CFO using $\hat{\theta}$ and $\tilde{\theta}$ in every DL slot.

E. PRACTICAL IMPLEMENTATION OF THE REAL-TIME OPERATING SFLC-OFDM SYSTEM

Several signal processing methods are proposed to attain channel reciprocity in previous sections. However, further considerations are required to implement the real-time operating SDR. In (13), (16) and (18), the involved estimates, namely phase rotation, offset, and residual CFO, are obtained through $\angle(\cdot)$. Thus, the normalization coefficient in average terms, i.e., $\frac{1}{63}$ in (11), and $\frac{1}{127}$ in (14) and (17), have no impact on the performance. By neglecting these coefficients, each average term in (11), (14), and (17) can be replaced by summation of received preamble symbols multiplied by conjugate of transmit preamble symbols so that the redundant division operations can be avoided. It is furthermore, considering that $S_k \in \{-1, 1\}$ for all k, only negation and addition are involved with the summation of the received preamble symbols, not multiplication and conjugate, resulting in the reduction of computation time for phase rotation estimation. Besides, $\bar{H}^{\mathrm{low}}$ and $\bar{H}^{\mathrm{up}}$ can be reused to compute the summation of received preamble CFR in (14) and (17) to avoid the redundant additions in the relative phase offset and fine CFO estimation. Algorithm 1 summarizes the implementation of phase rotation estimation.

As in Algorithm 1, the UL channel estimation with phase offset compensation can be implemented using the SIMD after phase rotation compensation. At first, the received pilot symbols and conjugate of transmit pilot symbols are put into two buffers. Then, least square channel estimation is conducted by applying the multiplication to these buffers with SIMD unit. After that, the relative phase offset is estimated from the received pilot symbols and stored to buffer. Then, the phase offset compensation is conducted with the SIMD by multiplying the buffer with the relative phase offset to the estimated channel. Implementation of UL channel estimation with SIMD is represented in Algorithm 2.

Theoretically, power normalization is required in SFLC encoding to meet the power constraint. However, an automatic gain controller controls TX power in a practical RF chain. Thus, the normalization $1/\sqrt{|H_{k,0}|^2 + |H_{k,1}|^2}$ in (1) is not necessary. By neglecting this term, unnecessary division operations can be avoided. Furthermore, since only multiplication and addition are involved in both SFLC encoding and decoding, these procedures can be implemented using the SIMD similarly with Algorithms 1 and 2.

To compensate the CFO, the phase shift corresponding to the frequency offset can be multiplied by the received signal in the time domain, which is referred to as the time-domain derotator [65, Ch. 6, pp. 158–159]. However, this method requires several multiplications, which is onerous to the real-time SDR implementation. For this reason, the CFO is

Algorithm 1 Implementation of Phase Rotation Estimation

Inputs: Received preamble symbols R_k.
Outputs: Phase rotation ϕ, sum of preamble CFR $\bar{H}$.
$\bar{H} \leftarrow 0$
for $k from -63 to 63$ **do**
  if $S_k > 0$ **then**
    $\bar{H} \leftarrow \bar{H} + R_k$.
  else
    $\bar{H} \leftarrow \bar{H} - R_k$.
  end if
  if $k = 0$ **then**
    $\bar{H}^{\mathrm{low}} \leftarrow \bar{H}$.
  end if
end for
$\bar{H}^{\mathrm{up}} \leftarrow \bar{H} - \bar{H}^{\mathrm{low}}$.
$\phi \leftarrow \frac{1}{64}\angle\left(\bar{H}^{\mathrm{up}}\bar{H}^{\mathrm{low},*}\right)$.

Algorithm 2 Implementation of UL Channel Estimation

Input: Received pilot symbol vector $\mathbf{q}_i$, transmit pilot conjugate vector $\mathbf{p}_i^*$, sum of preamble CFR $\bar{H}$.
Output: Estimated UL channel vector $\hat{\mathbf{h}}_i$.
Compensate the phase rotation of received pilot symbols based on Algorithm 1.
for $i from 0 to 1$ **do**
  $\tilde{H}_i \leftarrow 0$.
  for $m from 0 to |\mathcal{N}^{\mathrm{p}}|/L - 1$ **do**
    $\mathbf{b}_0 \leftarrow \mathbf{q}_i[mL : (m+1)L - 1]$.
    $\mathbf{b}_1 \leftarrow \mathbf{p}_i^*[mL : (m+1)L - 1]$.
    $\hat{\mathbf{h}}_i[mL : (m+1)L - 1] \leftarrow \mathbf{b}_1 \otimes \mathbf{b}_0$.
    $\tilde{H}_i \leftarrow \tilde{H}_i + \sum_{n=mL}^{(m+1)L-1} \hat{\mathbf{h}}_i[n]$.
  end for
end for
$H^{\mathrm{diff}} \leftarrow \tilde{H}_0^*\tilde{H}_1/|\tilde{H}_0^*\tilde{H}_1|$.
$\Psi_0^{\mathrm{UL}} \leftarrow \bar{H}/|\bar{H}|$.
$\Psi_1^{\mathrm{UL}} \leftarrow \Psi_0^{\mathrm{UL}}H^{\mathrm{diff}}$.
for $i from 0 to 1$ **do**
  $\mathbf{b}_2 \leftarrow \left[\Psi_i^{\mathrm{UL}}\ \Psi_i^{\mathrm{UL}}\ \ldots\ \Psi_i^{\mathrm{UL}}\right] \in \mathbb{C}^{1\times L}$.
  for $m from 0 to |\mathcal{N}^{\mathrm{p}}|/L - 1$ **do**
    $\mathbf{b}_3 \leftarrow \hat{\mathbf{h}}_i[mL : (m+1)L - 1]$.
    $\hat{\mathbf{h}}_i[mL : (m+1)L - 1] \leftarrow \mathbf{b}_3 \otimes \mathbf{b}_2$.
  end for
end for

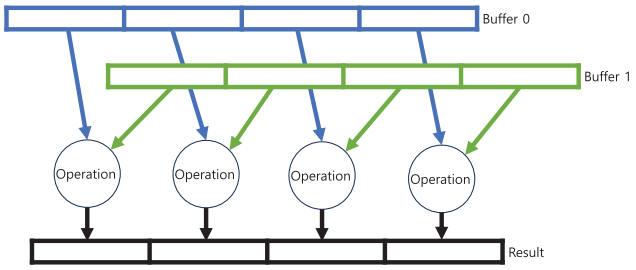

FIGURE 4. Illustration of SIMD executing the same four operations.

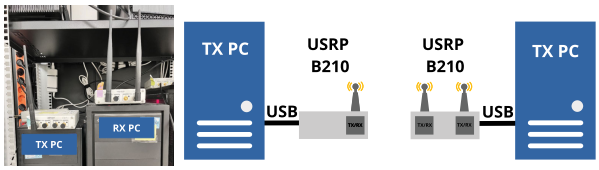

FIGURE 5. The testbed for experimental evaluation.

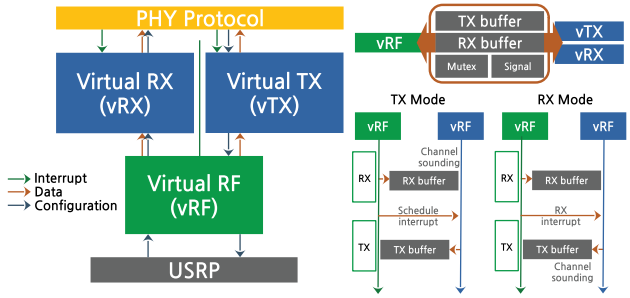

FIGURE 6. The architecture of the baseband software.

compensated by directly adjusting the carrier frequency of the USRP device in the SDR implementation. At the initial stage of communication, the estimate of the CFO can be substantial. Directly adjusting such a large frequency can make the RF chain unstable [80]. Thus, the UE compensates the CFO by fixed increment, not the estimated CFO. For the fast state transition from unlocked to locked, the increment value is set to relatively large at the unlocked state. While the small value of the increment is used at a locked state to avoid carrier frequency fluctuation.

IV. EXPERIMENTAL EVALUATION WITH A REAL-RIME TESTBED

For evaluating the performance of the proposed SFLC-OFDM system, we have implemented a testbed as depicted in Fig. 5. The testbed enables real-time channel estimation, SFLC transmission, and reception by utilizing signals transmitted over the air. Each node in the testbed serves as the BS or UE and consists of a PC running the necessary baseband software and a USRP B210 device. The USRP B210 device emits wireless signals generated by the baseband software and also samples and converts wireless signals into baseband signals which the baseband software can process. To ensure channel reciprocity, each USRP B210 device utilizes the same TX/RX

TABLE 1. The parameters of the experiments.

parameters	value
CPU	8th Generation Intel Core i7
CPU clock	3.70GHz
Center frequency	3300MHz
Sampling rate	15.36MHz
Bandwidth	10MHz
FFT size	1024
Subcarrier spacing	15kHz
N_{data}	600
Preamble sequence	M-sequence
N_p	127
N_D	4 (SSE 4.2)
Modulation	QPSK

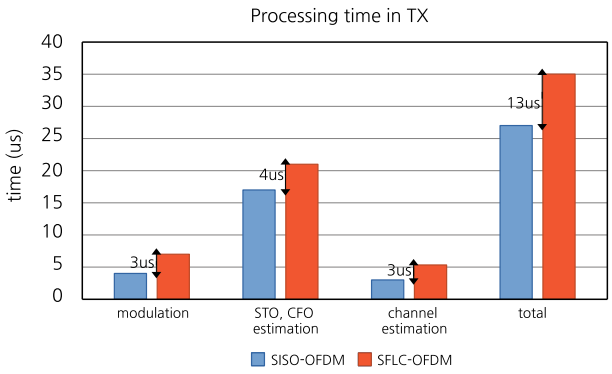

FIGURE 7. UL and DL processing time at the TX.

port for both DL and UL operations. This configuration ensures that both signal transmission and reception are performed using the same antenna and RF chain. Table 1 provides the configuration of the testbed hardware and the frame parameters used in the experiments.

The proposed signal processing methods are implemented on the baseband software. The overall architecture and interactions of the baseband software are illustrated in Fig. 6. The baseband software consists of three main threads: virtual TX (vTX), virtual RX (vRX), and virtual RF (vRF). The vRF thread controls the USRP B210 device, while the vTX and vRX threads handle signal processing at the baseband level. The vRF interacts with the vTX and vRX threads through TX and RX buffers. In the TX thread, the vTX processes the UL signal for channel estimation and generates the baseband signal for SFLC symbol transmission. Before SFLC encoding, the vTX derives $H_{k,0}$ and $H_{k,1}$ from the RX buffer, which contains the samples of the UL signal provided by the vRF.

The vTX then generates SFLC symbols based on $H_{k,0}$ and $H_{k,1}$ and stores them in the TX buffer. In the DL slot, the vRF passes the contents of the TX buffer to the USRP B210 device. The vRX handles the received baseband signal in the RX thread for SFLC symbol decoding. Additionally, for CSIT, the vRX generates the samples of the UL signal via the TX buffer. The vRF then passes these samples to the USRP B210 device to emit the signal in the UL slot.

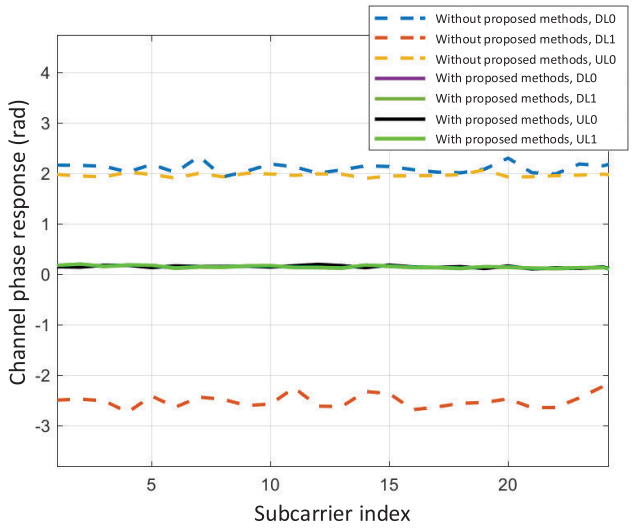

FIGURE 8. An example snapshot of the channel phase estimation.

A. THE UNIT-LEVEL PERFORMANCE OF THE PROPOSED METHODS

We first observe whether the proposed methods properly operate in real-time when implemented on the testbed. Fig. 7 depicts the measured processing time for the channel reciprocity recovery and SFLC encoding on the TX side. We compared the measured time of our implementation with a Single Input Single Output (SISO)-OFDM system without the proposed methods. Despite the proposed methods' additional compensation procedures, the overall signal processing time increase is approximately $13\mu s$. This amount of time can be effectively managed, considering the duration of the UL-to-DL switching time. The overall time for processing UL signals and generating SFLC symbols should be shorter than the UL-to-DL switching time. Based on the frame structure, the UL-to-DL switching time is $285\mu s$, corresponding to the duration of the 4 OFDM symbol, which is significantly larger than the time increment introduced by the proposed methods. The results thus demonstrate that the implementation can process the proposed methods in real-time. The results also indicate that the low-complexity designs of channel estimation and SFLC encoding contribute to the realization of the SFLC-OFDM system.

We then examine how the proposed methods recover phase reciprocity in a specific case. Fig. 8 presents an example of CFRs for 24 subcarriers, illustrating the significance of phase reciprocity recovery. In this experiment, BS temporarily transmits pilot symbols in DL slots so that UE can estimate DL CFR. Hence, $\hat{H}_{k,i}$ is estimated via UL signal processing at the BS, and $H_{k,i}$ is estimated via DL signal processing at the UE. The dashed line shows the observed CFRs at the antenna ports before the phase reciprocity recovery. The channel for each antenna port and subcarrier index experiences a different amount of phase rotation caused by residual timing offset and CFO, resulting in various phases across the antenna ports. This implies that the DL and UL CFRs phases are not identical. On the other hand, the CFRs observed after the phase reciprocity recovery, depicted as solid lines, remain consistent across both antenna ports and subcarrier indices.

This fact indicates effective compensation for the phase rotations caused by residual timing offset and CFO, and also validates the proper realization of channel reciprocity in the SFLC-OFDM system. The phase reciprocity recovery is essential for accurate channel estimation and data transmission with minimal distortion.

Finally, we assess the proposed methods' effectiveness from a statistical perspective. Fig. 9 illustrates the Normalized Mean Square Error (NMSE) for channel estimation obtained by the proposed methods across different SNR environments. The error is calculated during this evaluation by comparing the measured CSIT with the CSI measured at the RX. The results indicate that the error between the CSIs at the TX and RX decreases with increasing SNR. This observation indicates that the proposed methods effectively recover phase reciprocity from a functional perspective. Additionally, the NMSE becomes smaller than 1% and reaches a sufficiently low value when the SNR exceeds 10dB. This implies that the proposed methods reliably ensure phase reciprocity in the SFLC-OFDM system, particularly in moderate SNR regimes.

B. THE DECODING PERFORMANCE OF THE SFLC-OFDM SYSTEM

We evaluate the decoding performance of the proposed SFLC-OFDM system with the proposed methods at a system level. We compare it with the conventional SISO-OFDM system that utilizes CSI at the receiver. We also compare it with the SISO-OFDM system that utilizes CSIT based on the proposed signal processing methods. This comparison is for observing whether the channel reciprocity made by the proposed methods is valid for a SISO-OFDM environment.

In addition, we evaluate the decoding performance of various SFLC-OFDM systems. We compare the SFLC-OFDM systems with and without the proposed methods. This comparison will show how the proposed methods impact the overall decoding performance in an SFLC-OFDM environment. We also compare the SFLC-OFDM systems with and without amplitude calibration. SFLC encoding and decoding processes significantly depend on the ratio of $|H_{k,0}|$ and $|H_{k,1}|$. Therefore, the amplitude of CFRs for DL and UL should match so that the ratio of $|H_{k,0}|$ and $|H_{k,1}|$ is consistent for SFLC encoding and decoding processes. During the amplitude calibration, we adjust the gains of TX and RX chains for antenna ports so that the ratio of $|H_{k,0}|$ and $|H_{k,1}|$ is the same for DL and UL.

The quality of the symbol encoding and decoding is evaluated based on the error vector magnitude (EVM) of decoded symbols in the SFLC-OFDM system, defined as

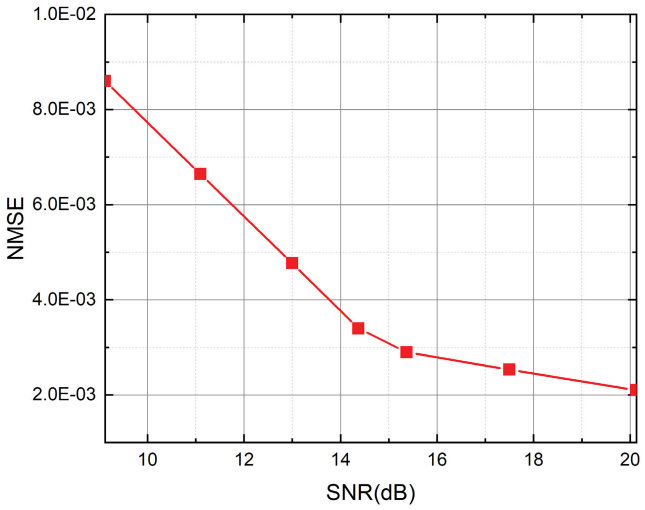

FIGURE 9. NMSE of the estimated CSI for DL and UL.

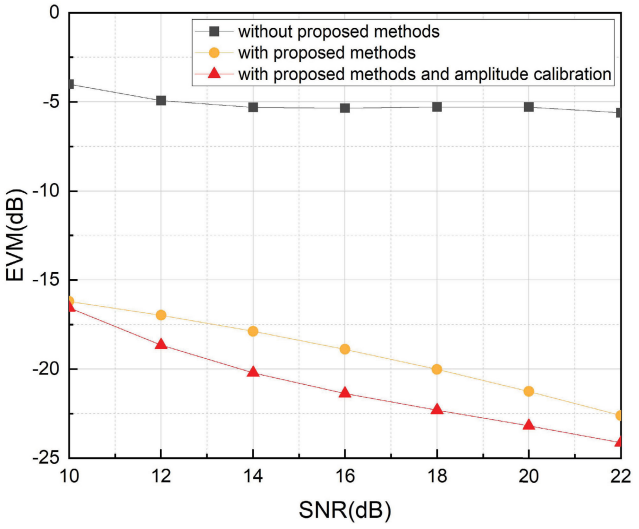

FIGURE 10. EVM of the decoded SFLC symbols.

follows:

$$EVM_{RMS} = \sqrt{E\left[\frac{\left|X_k - \hat{X}_k\right|^2}{|X_k|^2}\right]}. \tag{19}$$

Fig. 10 presents the measured EVM for 12,552 decoded symbols. If the proposed methods are not applied, the EVM does not sufficiently decrease, particularly in higher SNR regimes. However, when the proposed methods recover channel reciprocity, the EVM improves as SNR increases. These results demonstrate that the proposed methods for recovering phase reciprocity significantly enhance symbol accuracy. Furthermore, the results prove the necessity of amplitude calibration and the proposed methods. The amplitude calibration brings about 4dB SNR gain based on −20dB EVM.

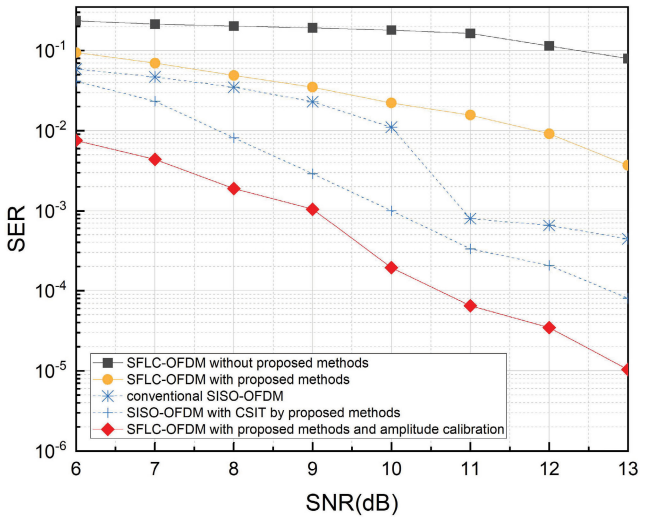

FIGURE 11. The SER for various systems.

Fig. 11 presents the Symbol Error Rate (SER) performance of the SFLC-OFDM and SISO-OFDM systems. The symbol error is determined by comparing the Maximum Likelihood (ML) hard-decision results and the transmitted symbols. The results show that the SFLC-OFDM systems without the proposed methods exhibit higher symbol error rates than the conventional SISO-OFDM systems. This highlights the significance of channel reciprocity in minimizing symbol errors. The non-reciprocal channel introduces impairment limiting the system's ability to gain full diversity. On the other hand, the SFLC-OFDM system with the proposed methods and amplitude calibration demonstrates lower symbol error rates and approaches the ideal performance. This indicates that the SFLC-OFDM system can gain sufficient diversity when both amplitude and phase reciprocities are achieved. Therefore, the proposed methods are significant to achieve the best performance regarding symbol error rate and obtain the potential diversity gain offered by SFLC.

Fig. 11 also presents the impact of the proposed methods on the performance of SISO-OFDM systems. If the SISO-OFDM system utilizes CSIT by the proposed methods, it performs significantly better than the conventional SISO-OFDM system with CSIR when the SNR is above 8.34 dB.

The enhanced performance is attributed to the proposed methods' accurate residual timing offset and CFO estimation. This consequently shows that the proposed methods can enhance error performance in other systems with various antenna configurations.

V. CONCLUSION

This paper presents the realization of an SFLC-OFDM system and illustrates the significance of the recovery of channel reciprocity to the SFLC-OFDM system. The SFLC-OFDM system designed in this paper establishes bidirectional channel symmetry between the DL and UL

and can utilize precise CSIT in the SFLC-OFDM system. It incorporates accurate synchronization methods in frequency and time domains to achieve phase reciprocity between DL and UL CFRs. For real-time signal processing, it also utilizes a low-complexity encoder and decoder capable of performing SFLC encoding and decoding within the UL-to-DL switching duration. The SFLC-OFDM system is implemented on a real-time operating testbed consisting of USRP B210s and PCs for performance evaluation. The experimental results obtained from the testbed demonstrate the successful restoration of channel reciprocity, as evidenced by achieving lower limits of EVM and SER performance in a practical implementation environment.

The realization of an SFLC-OFDM system can be a good guide for various MIMO systems utilizing CSIT. The proposed methods provide more accurate channel estimation in the SFLC-OFDM system and enhance overall system performance. For future works, this real-world implementation study can be extensively applied to large-scale MIMO systems encompassing multiple users. In addition, an automated calibration method needs to be investigated so that DL and UL channel gains are precisely and adaptively matched. The experimental results in this paper have presented that decoded symbols in the SFLC-OFDM system have significantly less EVM after rough recovery of amplitude reciprocity via the RF calibration. An advanced method that can estimate amplitude non-reciprocity more precisely would enable the system to compensate for the phase error of decoding symbols.

REFERENCES

[1] W. Saad, M. Bennis, and M. Chen, "A vision of 6G wireless systems: Applications, trends, technologies, and open research problems," *IEEE Netw.*, vol. 34, no. 3, pp. 134–142, May 2020.

[2] M. Giordani, M. Polese, M. Mezzavilla, S. Rangan, and M. Zorzi, "Toward 6G networks: Use cases and technologies," *IEEE Commun. Mag.*, vol. 58, no. 3, pp. 55–61, Mar. 2020.

[3] H. Tataria, M. Shafi, A. F. Molisch, M. Dohler, H. Sjöland, and F. Tufvesson, "6G wireless systems: Vision, requirements, challenges, insights, and opportunities," *Proc. IEEE*, vol. 109, no. 7, pp. 1166–1199, Jul. 2021.

[4] E. G. Larsson, O. Edfors, F. Tufvesson, and T. L. Marzetta, "Massive MIMO for next generation wireless systems," *IEEE Commun. Mag.*, vol. 52, no. 2, pp. 186–195, Feb. 2014.

[5] Y. Liqun, "Massive MIMO transmission technology for 6G," in *Proc. 19th Int. Comput. Conf. Wavelet Act. Media Technol. Inf. Process. (ICCWAMTIP)*, Chengdu, China, Dec. 2022, pp. 1–5.

[6] S. Suyama, T. Okuyama, N. Nonaka, and T. Asai, "Recent studies on massive MIMO technologies for 5G evolution and 6G," in *Proc. IEEE Radio Wireless Symp. (RWS)*, Las Vagas, NV, USA, Jan. 2022, pp. 90–93.

[7] Y. Chi, L. Liu, G. Song, Y. Li, Y. L. Guan, and C. Yuen, "Constrained capacity optimal generalized multi-user MIMO: A theoretical and practical framework," *IEEE Trans. Commun.*, vol. 70, no. 12, pp. 8086–8104, Dec. 2022.

[8] Z. Zhang, Y. Dong, K. Long, X. Wang, and X. Dai, "Decentralized baseband processing with Gaussian message passing detection for uplink massive MU-MIMO systems," *IEEE Trans. Veh. Technol.*, vol. 71, no. 2, pp. 2152–2157, Feb. 2022.

[9] A. Raafat, A. Agustin, and J. Vidal, "Downlink multi-user massive MIMO transmission using receive spatial modulation," *IEEE Trans. Wireless Commun.*, vol. 19, no. 10, pp. 6871–6883, Oct. 2020.

[10] R. Zhang, B. Shim, Y. Lou, S. Jia, and W. Wu, "Sparse vector coding aided ultra-reliable and low-latency communications in multi-user massive MIMO systems," *IEEE Trans. Veh. Technol.*, vol. 70, no. 1, pp. 1019–1024, Jan. 2021.

[11] J. Denis and M. Assaad, "Improving cell-free massive MIMO networks performance: A user scheduling approach," *IEEE Trans. Wireless Commun.*, vol. 20, no. 11, pp. 7360–7374, Nov. 2021.

[12] Y. Jiang and Y. Zou, "Secrecy energy efficiency maximization for multi-user multi-eavesdropper cell-free massive MIMO networks," *IEEE Trans. Veh. Technol.*, vol. 72, no. 5, pp. 6009–6022, May 2023.

[13] J. Zheng, J. Zhang, J. Cheng, V. C. M. Leung, D. W. K. Ng, and B. Ai, "Asynchronous cell-free massive MIMO with rate-splitting," *IEEE J. Sel. Areas Commun.*, vol. 41, no. 5, pp. 1366–1382, May 2023.

[14] H. A. Ammar, R. Adve, S. Shahbazpanahi, G. Boudreau, and K. V. Srinivas, "User-centric cell-free massive MIMO networks: A survey of opportunities, challenges and solutions," *IEEE Commun. Surveys Tuts.*, vol. 24, no. 1, pp. 611–652, 1st Quart., 2022.

[15] O. Elijah, C. Y. Leow, T. A. Rahman, S. Nunoo, and S. Z. Iliya, "A comprehensive survey of pilot contamination in massive MIMO—5G system," *IEEE Commun. Surveys Tuts.*, vol. 18, no. 2, pp. 905–923, 2nd Quart., 2016.

[16] K. Hassan, M. Masarra, M. Zwingelstein, and I. Dayoub, "Channel estimation techniques for millimeter-wave communication systems: Achievements and challenges," *IEEE Open J. Commun. Soc.*, vol. 1, pp. 1336–1363, 2020.

[17] X. Chen, D. W. K. Ng, W. Yu, E. G. Larsson, N. Al-Dhahir, and R. Schober, "Massive access for 5G and beyond," *IEEE J. Sel. Areas Commun.*, vol. 39, no. 3, pp. 615–637, Mar. 2021.

[18] J. Choi, D. J. Love, and P. Bidigare, "Downlink training techniques for FDD massive MIMO systems: Open-loop and closed-loop training with memory," *IEEE J. Sel. Topics Signal Process.*, vol. 8, no. 5, pp. 802–814, Oct. 2014.

[19] W. Shen, L. Dai, Y. Shi, B. Shim, and Z. Wang, "Joint channel training and feedback for FDD massive MIMO systems," *IEEE Trans. Veh. Technol.*, vol. 65, no. 10, pp. 8762–8767, Oct. 2016.

[20] J.-C. Shen, J. Zhang, E. Alsusa, and K. B. Letaief, "Compressed CSI acquisition in FDD massive MIMO: How much training is needed?" *IEEE Trans. Wireless Commun.*, vol. 15, no. 6, pp. 4145–4156, Jun. 2016.

[21] Y. Han, J. Lee, and D. J. Love, "Compressed sensing-aided downlink channel training for FDD massive MIMO systems," *IEEE Trans. Commun.*, vol. 65, no. 7, pp. 2852–2862, Jul. 2017.

[22] F. Rusek, D. Persson, B. K. Lau, E. G. Larsson, T. L. Marzetta, O. Edfors, and F. Tufvesson, "Scaling up MIMO: Opportunities and challenges with very large arrays," *IEEE Signal Process. Mag.*, vol. 30, no. 1, pp. 40–60, Jan. 2013.

[23] J. Hoydis, K. Hosseini, S. Ten Brink, and M. Debbah, "Making smart use of excess antennas: Massive MIMO, small cells, and TDD," *Bell Labs Tech. J.*, vol. 18, no. 2, pp. 5–21, Sep. 2013.

[24] H. Q. Ngo, E. G. Larsson, and T. L. Marzetta, "Energy and spectral efficiency of very large multiuser MIMO systems," *IEEE Trans. Commun.*, vol. 61, no. 4, pp. 1436–1449, Apr. 2013.

[25] Y. Nan, L. Zhang, and X. Sun, "Efficient downlink channel estimation scheme based on block-structured compressive sensing for TDD massive MU-MIMO systems," *IEEE Wireless Commun. Lett.*, vol. 4, no. 4, pp. 345–348, Aug. 2015.

[26] H. Q. Ngo and E. G. Larsson, "No downlink pilots are needed in TDD massive MIMO," *IEEE Trans. Wireless Commun.*, vol. 16, no. 5, pp. 2921–2935, May 2017.

[27] G. Liu, H. Deng, X. Qian, W. Wang, and G. Peng, "Joint pilot allocation and power control to enhance max-min spectral efficiency in TDD massive MIMO systems," *IEEE Access*, vol. 7, pp. 149191–149201, 2019.

[28] H. Lee, H. Choi, H. Kim, S. Kim, C. Jang, Y. Choi, and J. Choi, "Downlink channel reconstruction for spatial multiplexing in massive MIMO systems," *IEEE Trans. Wireless Commun.*, vol. 20, no. 9, pp. 6154–6166, Sep. 2021.

[29] J. W. Choi, B. Shim, and S.-H. Chang, "Downlink pilot reduction for massive MIMO systems via compressed sensing," *IEEE Commun. Lett.*, vol. 19, no. 11, pp. 1889–1892, Nov. 2015.

[30] J. Joung, "Space-time line code," *IEEE Access*, vol. 6, pp. 1023–1041, 2018.

[31] Y. Pang, Y. Xiao, X. Lei, and Y. Li, "Performance analysis and antenna selection for space time line code," *IEEE Access*, vol. 8, pp. 193503–193511, 2020.

[32] S.-C. Lim and J. Joung, "Transmit antenna selection for space-time line code systems," *IEEE Trans. Commun.*, vol. 69, no. 2, pp. 786–798, Feb. 2021.

[33] Y. Pang, Y. Xiao, X. Lei, and Y. L. Guan, "Performance analysis of space-time line code in correlated fading channels," *IEEE Trans. Veh. Technol.*, vol. 70, no. 6, pp. 6244–6248, Jun. 2021.

[34] S.-C. Lim and J. Joung, "Ergodic capacity of space-time line code systems with transmit antenna selection," *IEEE Trans. Veh. Technol.*, vol. 71, no. 8, pp. 9089–9094, Aug. 2022.

[35] R. Zedka, M. Bobula, J. Blumenstein, L. Polak, and M. Rupp, "Full-rate space-time line code with asymptotic SNR gain," *IEEE Commun. Lett.*, vol. 27, no. 5, pp. 1307–1311, May 2023.

[36] J. Joung, "Space-time line code for massive MIMO and multiuser systems with antenna allocation," *IEEE Access*, vol. 6, pp. 962–979, 2018.

[37] J. Joung and E.-R. Jeong, "Multiuser space-time line code with optimal and suboptimal power allocation methods," *IEEE Access*, vol. 6, pp. 51766–51775, 2018.

[38] J. Joung and J. Choi, "Multiuser space-time line code with transmit antenna selection," *IEEE Access*, vol. 8, pp. 71930–71939, 2020.

[39] J. Joung, J. Choi, and B. C. Jung, "Double space-time line codes," *IEEE Trans. Veh. Technol.*, vol. 69, no. 2, pp. 2316–2321, Feb. 2020.

[40] J. Choi and J. Joung, "Generalized space-time line code with receive combining for MIMO systems," *IEEE Syst. J.*, vol. 16, no. 2, pp. 1897–1908, Jun. 2022.

[41] J. Joung and J. Fan, "Linear precoding for space-time line code-based multicast systems," *IEEE Trans. Veh. Technol.*, vol. 71, no. 11, pp. 12386–12391, Nov. 2022.

[42] J. Choi, J. Joung, and B. C. Jung, "Space-time line code for enhancing physical layer security of multiuser MIMO uplink transmission," *IEEE Syst. J.*, vol. 15, no. 3, pp. 3336–3347, Sep. 2021.

[43] J. Choi, J. Joung, and Y.-S. Cho, "Artificial-noise-aided space-time line code for enhancing physical layer security of multiuser MIMO downlink transmission," *IEEE Syst. J.*, vol. 16, no. 1, pp. 1289–1300, Mar. 2022.

[44] J. Joung, "Energy efficient space-time line coded regenerative two-way relay under per-antenna power constraints," *IEEE Access*, vol. 6, pp. 47026–47035, 2018.

[45] J. Joung and J. Choi, "Space-time line codes with power allocation for regenerative two-way relay systems," *IEEE Trans. Veh. Technol.*, vol. 68, no. 5, pp. 4884–4893, May 2019.

[46] J. Joung, B. C. Jung, and J. Choi, "Space-time line coded regenerative two-way relay systems with power control," *Electron. Lett.*, vol. 55, no. 12, pp. 694–696, Jun. 2019.

[47] J. Youn, J. S. Yeom, J. Joung, and B. C. Jung, "Cooperative space-time line code for relay-assisted Internet of Things," *ICT Exp.*, vol. 9, no. 2, pp. 253–257, Apr. 2023.

[48] J. Kim, J. Joung, and K. Lim, "Intelligent reflecting surface-aided space-time line coded systems," *IEEE Wireless Commun. Lett.*, vol. 11, no. 2, pp. 245–249, Feb. 2022.

[49] J. Kim, J. Choi, J. Joung, and Y.-C. Liang, "Modified block coordinate descent method for intelligent reflecting surface-aided space-time line coded systems," *IEEE Wireless Commun. Lett.*, vol. 11, no. 9, pp. 1820–1824, Sep. 2022.

[50] H. Yu and J. Joung, "Frame structure design for vehicular-to-roadside unit communications using space-time line code under time-varying channels," *IEEE Syst. J.*, vol. 15, no. 2, pp. 3150–3153, Jun. 2021.

[51] J. Joung, H. Yu, and J. Zhao, "Bandwidth design for energy-efficient unmanned aerial vehicle using space-time line code," *IEEE Syst. J.*, vol. 15, no. 2, pp. 3154–3157, Jun. 2021.

[52] J. Joung and J. Fan, "Over-the-air computation strategy using space-time line code for data collection by multiple unmanned aerial vehicles," *IEEE Access*, vol. 9, pp. 105230–105241, 2021.

[53] J.-B. Seo, H. Jin, J. Joung, and B. C. Jung, "Uplink NOMA random access systems with space-time line code," *IEEE Trans. Veh. Technol.*, vol. 69, no. 4, pp. 4522–4526, Apr. 2020.

[54] K.-H. Lee, J. S. Yeom, J. Joung, and B. C. Jung, "Performance analysis of uplink NOMA with constellation-rotated STLC for IoT networks," *IEEE Open J. Commun. Soc.*, vol. 3, pp. 705–717, 2022.

[55] C. Wu, Y. Xiao, Y. L. Guan, J. Wang, X. Li, and P. Yang, "Space-time/frequency line coded OFDM: System design and practical implementation," *IEEE Access*, vol. 7, pp. 151915–151928, 2019.

[56] R. Rogalin, O. Y. Bursalioglu, H. C. Papadopoulos, G. Caire, and A. F. Molisch, "Hardware-impairment compensation for enabling distributed large-scale MIMO," in *Proc. Inf. Theory Appl. Workshop (ITA)*, Chengdu, China, Feb. 2013, pp. 1–10.

[57] W. Zhang, H. Ren, C. Pan, M. Chen, R. C. de Lamare, B. Du, and J. Dai, "Large-scale antenna systems with UL/DL hardware mismatch: Achievable rates analysis and calibration," *IEEE Trans. Commun.*, vol. 63, no. 4, pp. 1216–1229, Apr. 2015.

[58] M. Guillaud, D. T. M. Slock, and R. Knopp, "A practical method for wireless channel reciprocity exploitation through relative calibration," in *Proc. 8th Int. Symp. Signal Process.*, vol. 1, Aug. 2005, pp. 403–406.

[59] F. Kaltenberger, H. Jiang, M. Guillaud, and R. Knopp, "Relative channel reciprocity calibration in MIMO/TDD systems," in *Proc. Future Netw. Mobile Summit*, Florence, Italy, Jun. 2010, pp. 1–10.

[60] C. Shepard, H. Yu, N. Anand, E. Li, T. Marzetta, R. Yang, and L. Zhong, "Argos: Practical many-antenna base stations," in *Proc. 18th Annu. Int. Conf. Mobile Comput. Netw.*, Istanbul, Turkey, Aug. 2012, pp. 53–64.

[61] X. Jiang, M. Cirkic, F. Kaltenberger, E. G. Larsson, L. Deneire, and R. Knopp, "MIMO-TDD reciprocity under hardware imbalances: Experimental results," in *Proc. IEEE Int. Conf. Commun. (ICC)*, JLondon, U.K., Jun. 2015, pp. 4949–4953.

[62] T. Magounaki, F. Kaltenberger, X. Jiang, C. Buey, P. Ratajczak, and F. Ferrero, "Experimental evaluation of relative calibration in a MISO-TDD system," in *Proc. Eur. Conf. Netw. Commun. (EuCNC)*, Oulu, Oulu, Finland, Jun. 2017, pp. 1–5.

[63] T. Magounaki, F. Kaltenberger, and R. Knopp, "Real-time performance evaluation of relative calibration on the OAI 5G testbed," in *Proc. 53rd Asilomar Conf. Signals, Syst., Comput.*, Pacific Grove, CA, USA, Nov. 2019, pp. 564–568.

[64] T. Magounaki, F. Kaltenberger, and R. Knopp, "Modeling the distributed MU-MIMO OAI 5G testbed and group-based OTA calibration performance evaluation," in *Proc. IEEE 21st Int. Workshop Signal Process. Adv. Wireless Commun. (SPAWC)*, May 2020, pp. 1–5.

[65] T.-D. Chiueh, P.-Y. Tsai, and I.-W. Lai, *Baseband Receiver Design for Wireless MIMO-OFDM Communications*, 2nd ed. Hoboken, NJ, USA: Wiley, 2012.

[66] P. Tan and N. C. Beaulieu, "Effect of channel estimation error on bit error probability in OFDM systems over Rayleigh and Ricean fading channels," *IEEE Trans. Commun.*, vol. 56, no. 4, pp. 675–685, Apr. 2008.

[67] *NR; Physical Channels and Modulation*, document TS 38.211 v15.10.0, 3GPP, Jul. 2018.

[68] S. Huang, Y. Su, Y. He, and S. Tang, "Joint time and frequency offset estimation in LTE downlink," in *Proc. 7th Int. Conf. Commun. Netw. China*, Kun Ming, China, Aug. 2012, pp. 394–398.

[69] S. Coleri, M. Ergen, A. Puri, and A. Bahai, "Channel estimation techniques based on pilot arrangement in OFDM systems," *IEEE Trans. Broadcast.*, vol. 48, no. 3, pp. 223–229, Sep. 2002.

[70] Y. S. Cho, J. Kim, W. Yang, and C. G. Kang, *MIMO-OFDM Wireless Communications With MATLAB*, 1st ed. Hoboken, NJ, USA: Wiley, 2010.

[71] A. Mohammadian and C. Tellambura, "RF impairments in wireless transceivers: Phase noise, CFO, and IQ imbalance—A survey," *IEEE Access*, vol. 9, pp. 111718–111791, 2021.

[72] A. Bourdoux, B. Come, and N. Khaled, "Non-reciprocal transceivers in OFDM/SDMA systems: Impact and mitigation," in *Proc. Radio Wireless Conf.*, Boston, MA, USA, Aug. 2003, pp. 183–186.

[73] D.-C. Chang, "Effect and compensation of symbol timing offset in OFDM systems with channel interpolation," *IEEE Trans. Broadcast.*, vol. 54, no. 4, pp. 761–770, Dec. 2008.

[74] S. Wu and Y. Bar-Ness, "OFDM channel estimation in the presence of frequency offset and phase noise," in *Proc. IEEE Int. Conf. Commun.*, Anchorage, AK, USA, May 2003, pp. 3366–3370.

[75] N. Nikaein, R. Knopp, F. Kaltenberger, L. Gauthier, C. Bonnet, D. Nussbaum, and R. Ghaddab, "Demo: OpenAirInterface: An open LTE network in a PC," in *Proc. 20th Annu. Int. Conf. Mobile Comput. Netw.*, Maui, HI, USA, Sep. 2014, pp. 305–308.

[76] X. Wang, C. Wang, X. Li, W. Wang, and Y. Zhang, "Design and implementation of the NB-IoT downlink system on OpenAirInterface platform," in *Proc. IEEE 4th Int. Conf. Comput. Commun. (ICCC)*, Chengdu, China, Dec. 2018, pp. 880–884.

[77] S. Tretter, "Estimating the frequency of a noisy sinusoid by linear regression (Corresp.)," *IEEE Trans. Inf. Theory*, vol. IT-31, no. 6, pp. 832–835, Nov. 1985.

[78] Y.-H. You, J. Kim, and H.-K. Song, "Pilot-assisted fine frequency synchronization for OFDM-based DVB receivers," *IEEE Trans. Broadcast.*, vol. 55, no. 3, pp. 674–678, Sep. 2009.
[79] D. Zhang, Y. Hu, Y. Chen, and B. Zeng, "Calibrating phase offsets for commodity WiFi," *IEEE Syst. J.*, vol. 14, no. 1, pp. 661–664, Mar. 2020.
[80] B. Razavi, "Design considerations for direct-conversion receivers," *IEEE Trans. Circuits Syst. II, Analog Digit. Signal Process.*, vol. 44, no. 6, pp. 428–435, Jun. 1997.

SUBIN KIM received the B.S. and M.S. degrees in electronics engineering from Sookmyung Women's University, Seoul, South Korea, in 2022 and 2023, respectively. Her current research interests are signal processing and next-generation wireless communication.

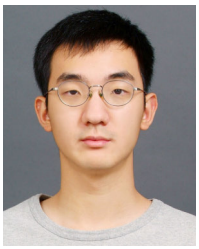

HAN-GYEOL LEE (Student Member, IEEE) received the B.S. and M.S. degrees in electrical and electronics engineering from Chung-Ang University (CAU), Seoul, South Korea, in 2021 and 2023, respectively. His current research interests include signal processing and physical layer design for next-generation wireless networks.

SONGMIN LEE received the B.S. degree in electronics engineering from Sookmyung Women's University, Seoul, South Korea, in 2023, where she is currently pursuing the M.S. degree in electronics engineering. Her current research interests are signal processing and software modem development.

JAEHONG KIM (Student Member, IEEE) received the B.S. and M.S. degrees in electrical and electronics engineering from Chung-Ang University, Seoul, South Korea, in 2021 and 2023, respectively, where he is currently pursuing the Ph.D. degree with the Department of Electrical and Electronics Engineering. His areas of interests include space–time coding, intelligent reflecting surface, and wireless communications with machine learning.

JINGON JOUNG (Senior Member, IEEE) received the B.S. degree in radio communication engineering from Yonsei University, Seoul, South Korea, in 2001, and the M.S. and Ph.D. degrees in electrical engineering and computer science from KAIST, Daejeon, South Korea, in 2003 and 2007, respectively.

He was a Postdoctoral Fellow with KAIST, and UCLA, CA, USA, in 2007 and 2008, respectively. He was a Scientist with the Institute for Infocomm Research, Singapore, from 2009 to 2015, and joined Chung-Ang University (CAU), Seoul, in 2016, as a Faculty Member. He is currently a Professor with the School of Electrical and Electronics Engineering, CAU, where he is also the Principal Investigator of the Intelligent Wireless Systems Laboratory. His research interests include signal processing, numerical analysis, algorithms, and machine learning.

Dr. Joung is an inventor of a Space-Time Line Code (STLC), that is a fully symmetric scheme to a Space-Time Block Code. He was recognized as an Exemplary Reviewer of the IEEE Communications Letters, in 2012, and the IEEE Wireless Communications Letters, from 2012 to 2014 and in 2019. He served as a Guest Editor for IEEE Access, in 2016. He served as a Editorial Board Member for the *APSIPA Transactions on Signal and Information Processing*, from 2014 to 2019; a Guest Editor for the *Electronics*, in 2019; and an Associate Editor for IEEE Transactions on Vehicular Technology, from 2018 to 2023.

JUYEOP KIM (Member, IEEE) received the B.S. and Ph.D. degrees in electrical engineering from the Korea Advanced Institute of Science and Technology (KAIST), in 2004 and 2010, respectively. He is an Assistant Professor with the Department of Electronics Engineering, Sookmyung Women's University, Seoul, South Korea. His current research interests are software modems and next-generation wireless communication.